ELSEVIER

Ceramics International 32 (2006) 43–51

CERAMICS INTERNATIONAL

www.elsevier.com/locate/ceramint

Crystallisation behaviour, microstructure and magnetic properties of $BaO–Fe_2O_3–B_2O_3–SiO_2$ glass ceramics

M. Mirkazemi *, V.K. Marghussian, A. Beitollahi

Ceramics Division, Department of Materials, Iran University of Science and Technology, Narmak, Tehran 16844, Iran

Received 22 September 2004; received in revised form 2 November 2004; accepted 20 December 2004
Available online 29 April 2005

Abstract

Differential thermal analysis, X-ray diffractometry and scanning electron microscopy with energy dispersive spectroscopy were used to study the crystallisation of glass ribbons with a composition of 35% BaO, 35%Fe_2O_3, 20%B_2O_3 and 10% SiO_2 (mol%) prepared via cooling the melts between steel rollers. The magnetic properties of specimens were also measured with a vibrating sample magnetometer.

Heat treatment of glass specimens both in the form of bulk (ribbon) or pressed powders at their respective DTA exo-peak temperatures of 722 and 702 °C led to the formation of $BaFe_{12}O_{19}$ and BaB_2O_4 as the only crystalline phases. The pressed powders showed the finest and the broadest size distribution of acicular and platelet particles in the 0.1–2.5 μm range. The glass ribbons heat treated in one-stage exhibited the most uniform distribution of platelet particles of 0.9 μm mean size, while a two-stage heat treatment led to a bimodal size distribution of platelet particles. All specimens showed nearly identical values of saturation magnetisation of M_s = 25–27 emu/g while the coercivity values varied between H_c = 2800–3800 Oe.

Keywords: C. Magnetic properties; D. Glass ceramic; D. Ferrites; E. Hard magnets

1. Introduction

The glass crystallisation method has been widely used to synthesise various magnetic materials, especially barium hexaferrites, in recent years.

Barium hexaferrites owing to their superior properties have been utilised in various applications as permanent magnets and particulate media for recording high density information. Most investigators have chosen B_2O_3 as a glass former for their base glass compositions which are mainly located in the $BaO–Fe_2O_3–B_2O_3$ system. Many aspects of the process, including the effect of composition, nucleating agents and heat treatment schedule upon magnetic properties have been reported [1–12].

Borate glass offers many advantages in this process, especially for manufacturing particulate recording media, where the amorphous phase must be leached out and the inherent low chemical durability of borate glasses facilitate the process. However, for other applications, e.g. thin films, where the magnetic phase should be dispersed in a glassy matrix, the glass should be chemically more resistant and not vulnerable to moisture attack. There have been some attempts to change the properties of matrix glasses by partially replacing B_2O_3 by other oxides or by application of different glass forming systems [9,12–15]. The present authors have shown [16] that it is possible to replace B_2O_3 by 10 mol% SiO_2 in the composition $0.45BaO·0.25Fe_2O_3·0.30B_2O_3$. It was supposed that in addition to improve the durability of glass, this could also decrease the crystallisation rate of the melt and make it more controlable. However, it was proved that the resultant glass-ceramics while showing a relatively high coercivity exhibited a low value of saturation magnetisation. This was attributed to the relatively low content of magnetic phase. In the present study it was decided to raise the content of hexaferrite phase by increasing the Fe_2O_3 content at the

* Corresponding author. Tel.: +98 21 745 1500–10; fax: +98 21 745 4057.
E-mail address: mirkazemi@mail.iust.ac.ir (M. Mirkazemi).

0272-8842/$30.00
doi:10.1016/j.ceramint.2004.12.008

Table 1
Chemical composition of glass samples

	Chemical composition (mol%)			
	BaO	Fe_2O_3	B_2O_3	SiO_2
Base composition	45	25	20	10
F_{30}	40	30	20	10
F_{33}	37	33	20	10
F_{35}	35	35	20	10
F_{40}	30	40	20	10
F_{45}	25	45	20	10
F_{50}	20	50	20	10

expense of BaO and to investigate the crystallisation behaviour, microstructure and magnetic properties of the resultant glasses.

2. Experimental procedure

Table 1 shows the compositions of the selected glasses. The glasses were prepared by melting the required amounts of reagent grade chemicals ($BaCO_3$, H_3BO_3, Fe_2O_3 and a very pure quartz sand) in alumina crucibles at 1300–1460 °C for 1 h in an electrically heated furnace. In order to prevent the crystallisation of the high iron glasses the melts were quenched between two steel rollers.

Using this process ribbon samples of ~70 μm in thickness were obtained. To verify the amorphous nature of the samples they were analyzed by X-ray diffractometry (XRD) (Philips model PW3710 using Co Kα radiation).

Differential thermal analysis (DTA) (Stanton Redcraft model STA-780) was utilised to determine the glass transition temperature (T_g), dilatometric softening point (T_d) and crystallisation temperature (T_c) of the glass samples. The heating rate was 20 °C min^{-1} and alumina was used as an inert reference material. The shifts of crystallisation (exothermic) peaks (ΔT values) upon changing the DTA sample particle sizes in the <53 μm to the 0.5–0.6 mm range were also measured. The particle sizes were determined utilizing standard sieves.

The samples were then heat treated at their corresponding crystallisation temperatures for different time periods and the crystalline phases developed after heat treatment were identified by XRD. The microstructures were observed with a scanning electron microscope (Cambridge SEM model 360). Two sets of specimens were used, bulk (in the form of ribbons) and glass powders. The latter specimens were prepared by pressing the glass powders (<53 μm) at 130 MPa into cylinders of 1 cm in diameter and 2 cm in height. To prepare the SEM specimens the pressed specimens were polished and etched in 0.5% HF for 75 s and the bulk specimens (ribbons) were directly etched in HF solution for 2.5 min without polishing. Both specimens were coated with a thin film of gold prior to the microstructural examinations. The saturation magnetisation (M_s) and coercivity (H_c) were determined with a vibrating sample magnetometer.

3. Results and discussion

3.1. Prepared glasses

Table 1 shows the glass compositions investigated in this work. As discussed elsewhere [16] 10 wt.% SiO_2 was added to the composition $0.45BaO{\cdot}0.25Fe_2O_3{\cdot}0.30B_2O_3$ (at the expense of B_2O_3) in order to enhance the chemical durability and reduce the crystallisation rate. Owing to the relatively low content of iron oxide in this base composition, the theoretical yield of hexaferrite was anticipated to be only ~36 wt.%, giving rise to a M_s value of as low as 9.92 emu/g [16]. Specimens F_{30}–F_{50} were formulated by replacing BaO by Fe_2O_3 in the base composition. The well known limitation of this displacement process is the possibility of precipitation of iron oxides from melts during quenching operation which is undesirable. Fig. 1 shows the XRD results of as quenched glass specimens. It can be seen that the addition of Fe_2O_3 only up to ~35 wt.% is permissible. Above this limit the precipitation of Fe_2O_3 and Fe_3O_4 phases was detectable. Therefore, the specimen containing 35 wt.% Fe_2O_3 (F_{35}) was adopted as the most suitable specimen and was used in all remaining experiments.

3.2. Differential thermal analysis and crystallisation products

As the DTA traces shown in Fig. 2 indicate, the sample F_{35} having a coarse particle size exhibited a very weak exothermic peak (at 722 °C), whereas the specimen with a finer particle size presented two distinct exothermal effects at 603 and 702 °C. This fact along with the relatively large DTA peak shift of the fine particle size specimen relative to the coarse particle size specimen ($\Delta T = 20$) can be taken as an indication of a tendency towards surface crystallisation. Table 2 summarises the DTA results and Table 3 shows the crystallisation products after heat treating the samples at their respective DTA exo-peak temperatures for the indicated time periods. It must be mentioned that specimen D was a bulk glass sample (similar to C) that was subjected to a two-stage heat treatment schedule (nucleation and growth). The nucleation temperature (527 °C) was chosen half-way between T_g and T_d temperatures. It can be concluded that in the case of specimen B (which was in the form of compacted glass particles) the prevalence of BaB_2O_4 phase over $BaFe_{12}O_{19}$ is owing to the greater tendency of the former phase towards surface crystallisation. In the case of specimen C (having a bulk form) this tendency has been suppressed and in specimen D the nucleation step probably has assisted the bulk crystallisation of BaB_2O_4. It is interesting to note that the amount of $BaFe_{12}O_{19}$ was apparently not affected by the surface area or details of heat

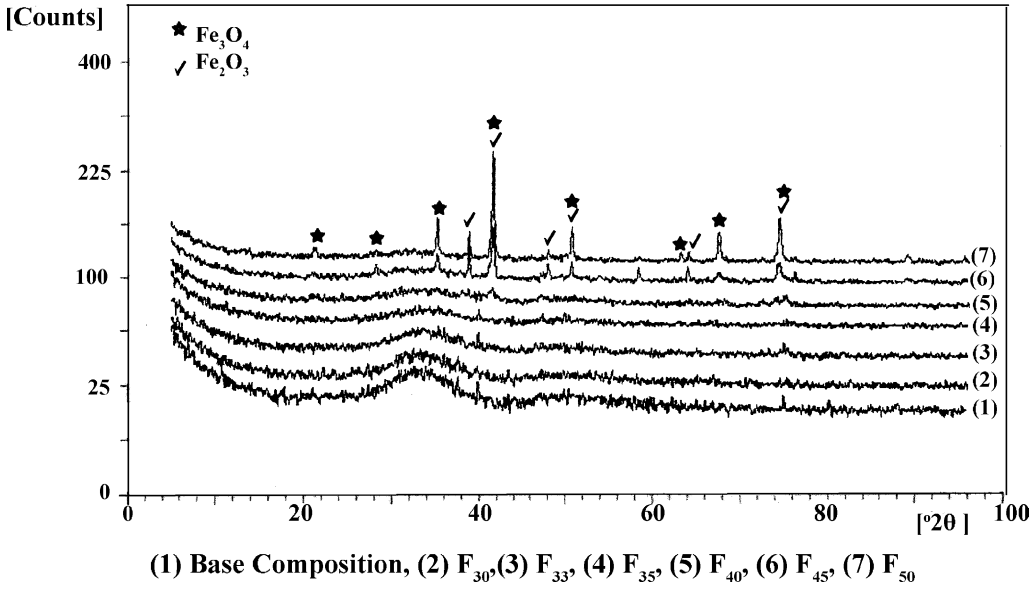

Fig. 1. XRD patterns for as quenched glasses.

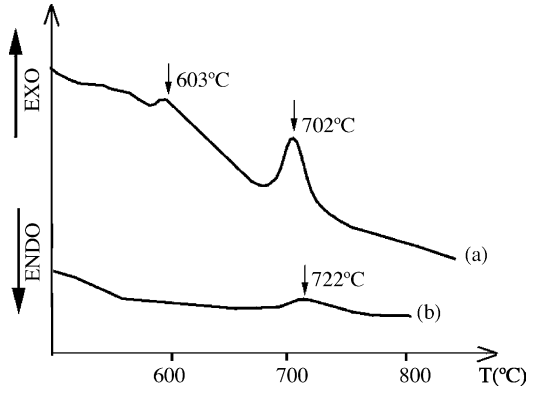

Fig. 2. DTA traces for specimen F_{35}: (a) fine particle size (<53 μm) and (b) coarse particle size (0.5–0.6 mm).

Table 2
DTA Characteristic temperatures of glasses (°C)

Glass sample	T_g	T_d	T_c
Fine	513	540	603 and 702
Coarse	513	548	722

treatment schedule used in this work. Fig. 3 depicts some XRD results.

3.3. Microstructural investigations

Figs. 4–9 represent SEM micrographs of some specimens. It can be seen that specimen B exhibited a quite non-uniform microstructure regarding the size and shape of crystallised particles (Fig. 4). Some particles have apparently grown as needles while others represent platelet morphology (white phase in Fig. 5). The particles with both morphologies can be assigned to $BaFe_{12}O_{19}$ phase as proved by energy dispersive spectroscopy (EDS). Fig. 5 also reveals the possible sequence of the crystallisation process in this specimen. It seems that BaB_2O_4 is the first major phase that has been crystallised (grey phase). $BaFe_{12}O_{19}$ particles subsequently were crystallised within the BaB_2O_4 rich regions which serve as suitably heterogeneous nucleation sites for their formation. The great tendency of BaB_2O_4 for surface crystallisation and the high intensity of this phase in XRD patterns (as discussed before) support this postulate. The $BaFe_{12}O_{19}$ crystallisation by reaction of BaB_2O_4 and Fe_2O_3 (from glassy phase) has been reported by many investigators [5,17]. It seems that in the present work the $BaFe_{12}O_{19}$ particles that have grown directly from the glass

Table 3
Heat treatment conditions and crystallisation results

Sample	Grain size	Heat treatment temperature (°C)	Heat treatment time (h)	Crystallisation products
A	Powder (<53 μm)	603	1	$BaFe_{12}O_{19}$ (VW)
B	powder (<53 μm)	702	1	$BaFe_{12}O_{19}$ (S)/BaB_2O_4 (VS)
C	Bulk	722	1	$BaFe_{12}O_{19}$ (S)/BaB_2O_4 (VW)
D	Bulk	527 and 722	1 and 1	$BaFe_{12}O_{19}$ (S)/BaB_2O_4 (S)

X-ray diffraction intensities are written in parentheses: VW, very weak; S, strong; VS, very strong.

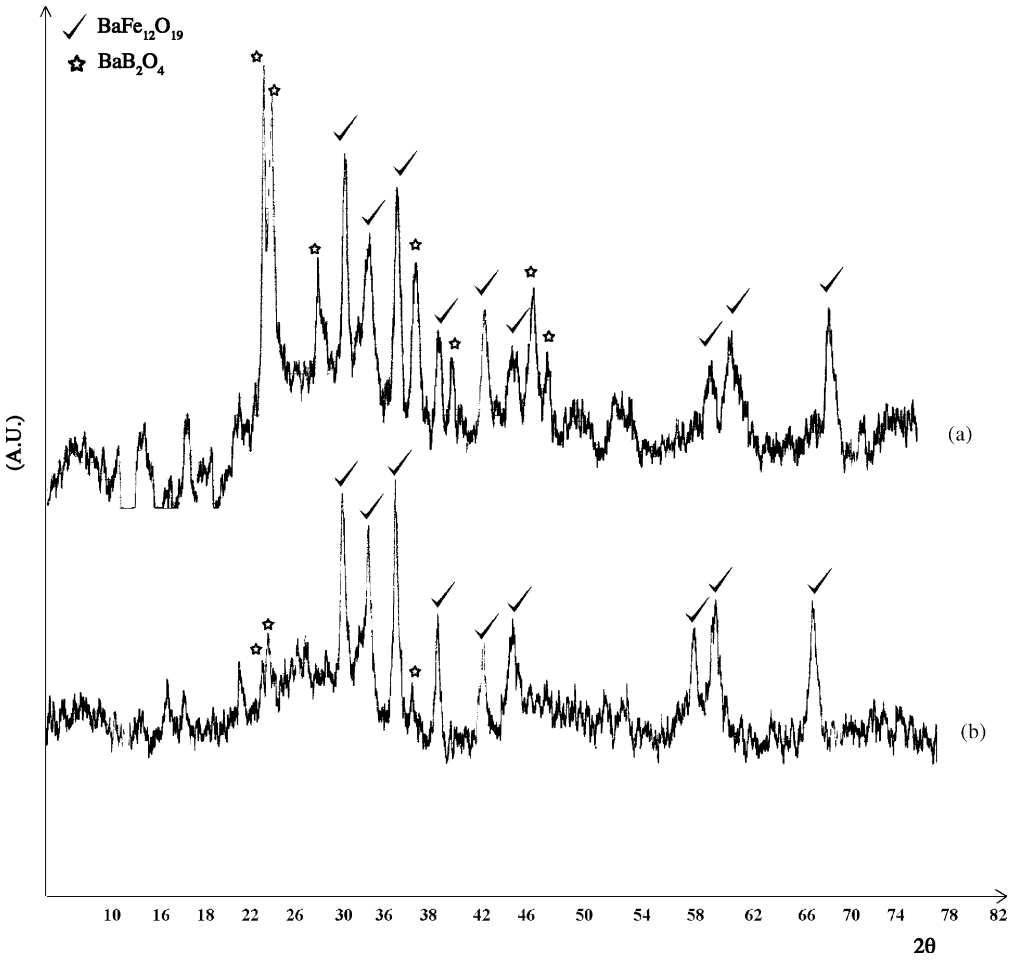

Fig. 3. XRD patterns for (a) specimen B, (b) specimen C.

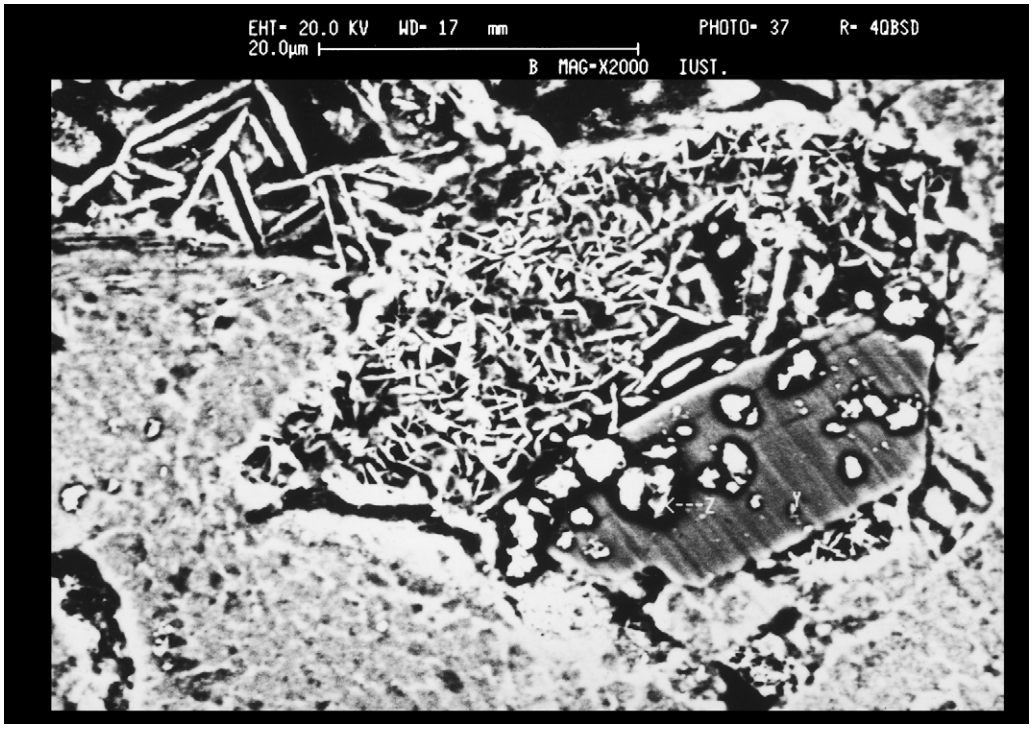

Fig. 4. SEM micrograph of specimen B showing several varieties of $BaFe_{12}O_{19}$ particles.

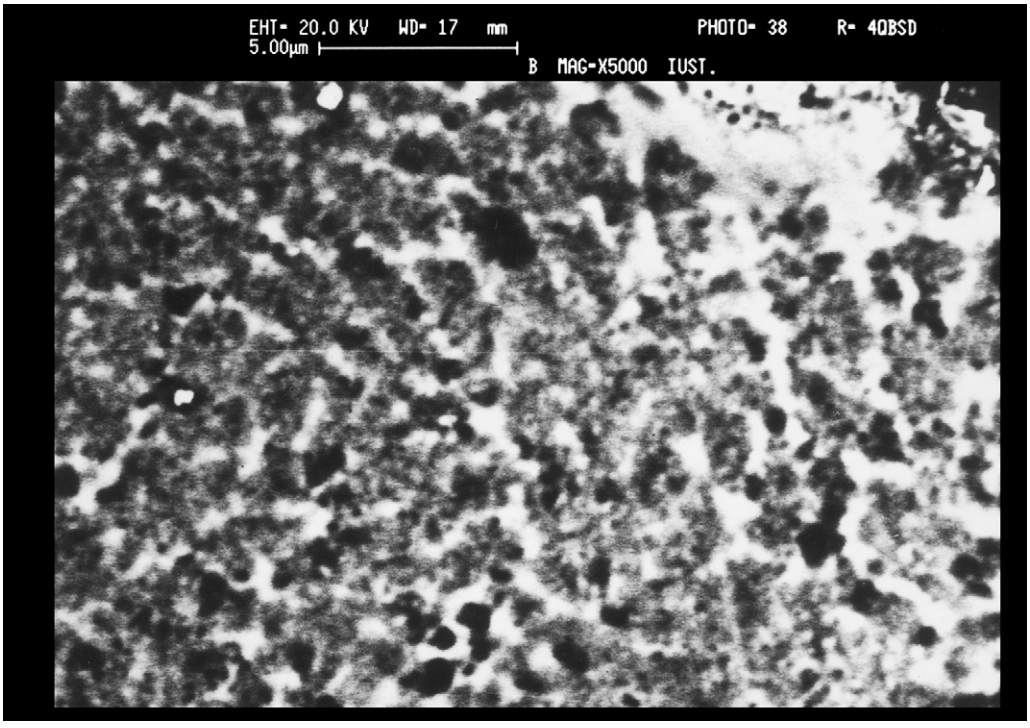

Fig. 5. Enlarged micrograph of specimen B showing platelets of $BaFe_{12}O_{19}$ (white phase) growing within grey phase (BaB_2O_4).

surface were more probable to have an acicular morphology, while the particles grown on the previously crystallized BaB_2O_4 (or $BaFe_{12}O_{19}$) particles mostly exhibited a platelet morphology.

Fig. 4 also depicts a well developed crystal of $BaFe_{12}O_{19}$, clearly exhibiting the hexagonal habit. It can probably be attributed to the secondary growth of some occasional nuclei or very tiny crystalline clusters formed during cooling of the initial melt which were not detectable by XRD. These crystals can be served as suitable sites for nucleation of new hexaferrite crystals in the later stages of heat treatment as shown in Fig. 4.

Fig. 6 represents the microstructure of specimen C. In this bulk glass-ceramic the hexaferrite phase exhibits a quite

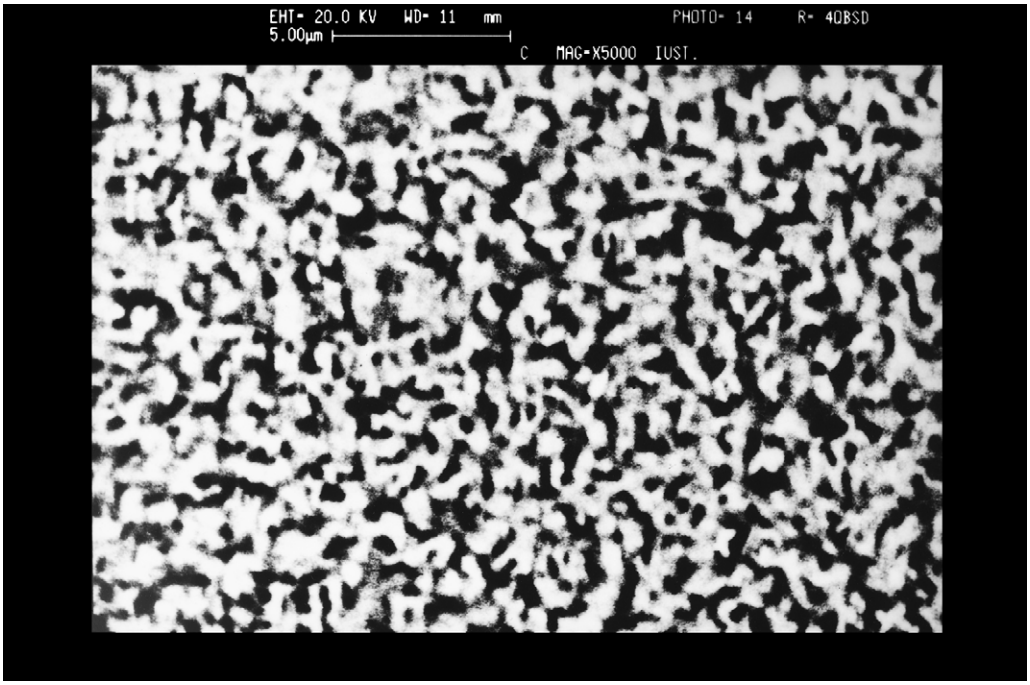

Fig. 6. SEM micrograph of specimen C showing the uniform distribution of $BaFe_{12}O_{19}$ platelets.

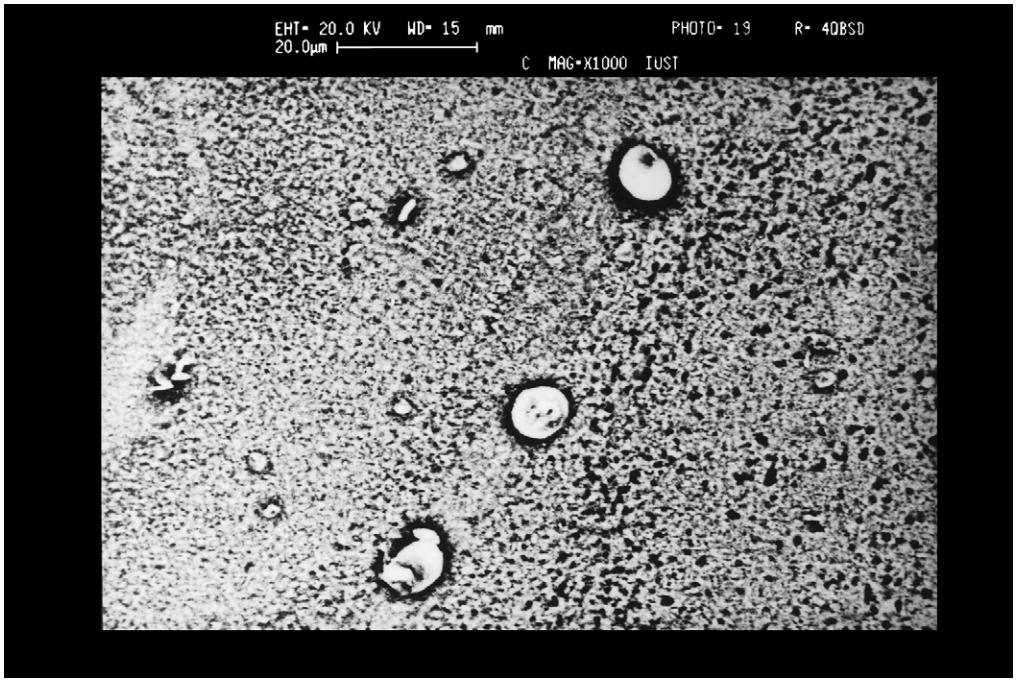

Fig. 7. SEM micrograph of specimen C showing spherical particles of BaB_2O_4 phase.

uniform distribution of platelet particles with a mean size of ~0.9 μm, while BaB_2O_4 phase has appeared as some isolated spherical particles as shown in Fig. 7. These particles seem to be formed by a spherulitic growth process as discussed elsewhere [16]. In specimen D, which has nucleated at 527 °C, for 1 h prior to the final crystallisation at 722 °C, some well grown hexagonal ferrite particles have appeared with a mean diameter of ~14 μm (Fig. 8). It seems that these particles have been originated from the nuclei formed during the first step of the heat treatment process. Their formation can be explained as follows: during quenching of the glassy ribbons, or their subsequent heating up, probably some nuclei have been formed within amorphous specimens which have served as crystallisation

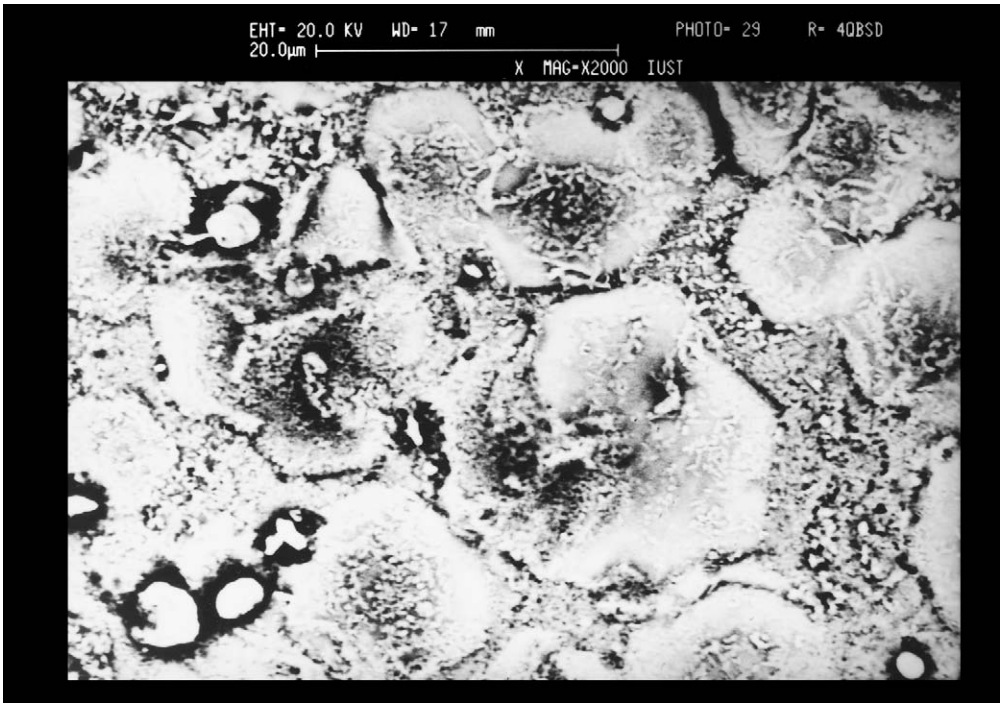

Fig. 8. SEM micrograph of specimen D showing well grown hexagonal particles of $BaFe_{12}O_{19}$ particles.

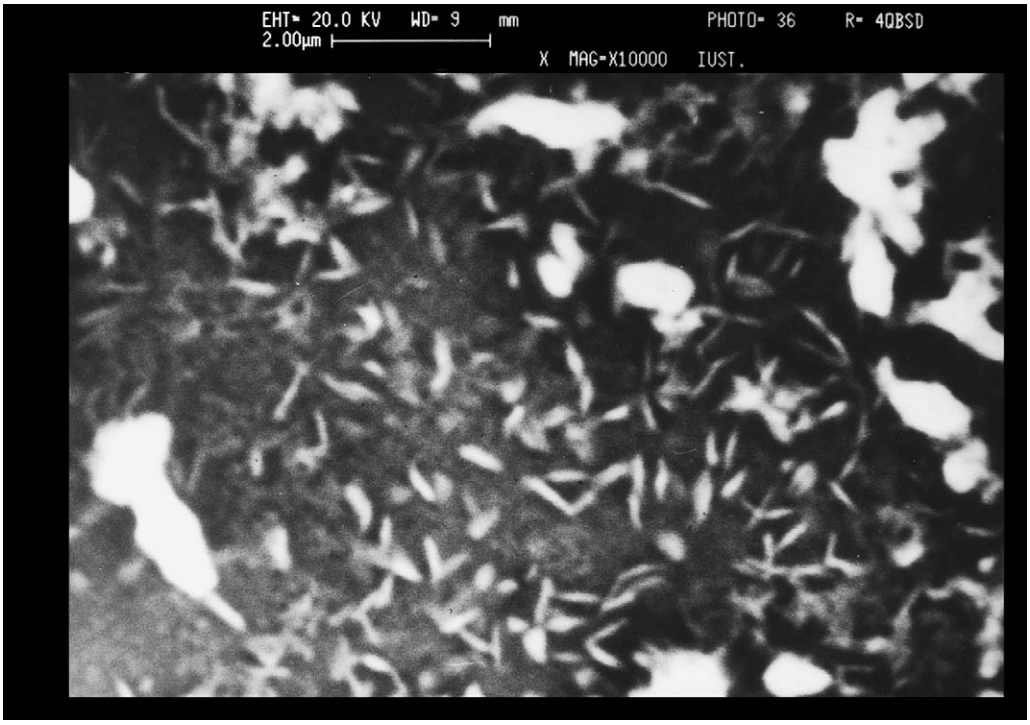

Fig. 9. Enlarged SEM micrograph of specimen D showing tiny $BaFe_{12}O_{19}$ platelets growing on the previously formed hexagonal particles (background).

sites for specimen C during 1 h hold at the growth temperature, giving rise to a relatively uniform microstructure of fine platelet particles. Whereas in the case of specimen D, the 1 h hold at 527 °C perhaps has led to the coarsening of the pre-existing nuclei (fewer and larger particles) and less efficient nucleation. Owing to the existence of fewer nuclei in specimen D, the particles have grown to quite big sizes during the second stage of heat treatment at 722 °C.

In Fig. 8 also a great number of very tiny particles can be observed growing on the previously formed hexagonal particles. The enlarged picture shown in Fig. 9 reveals the platelet morphology of these particles with a mean size of ~0.6 μm. Meanwhile in specimen D the spherical barium borate (BaB_2O_4) particles has formed in greater numbers as compared with specimen C. This is an indication that the nucleation step probably assisted the crystallisation of the borate phase in bulk specimens. The spherulitic growth morphology usually is encountered in conditions when sufficient nuclei are not present [18,19]. Therefore, the absence of borate spherulites in specimen B and the occurrence of a quite different crystallisation mechanism and morphology for their formation can be attributed to the prevalence of surface crystallisation of the borate phase in these specimens.

3.4. Magnetic properties

Table 4 summarises the magnetic properties of prepared specimens. It can be seen that the three specimens show approximately the same value of saturation magnetisation (25–27 emu/g).

Considering the fact that the content of iron oxide determines the amount of $BaFe_{12}O_{19}$ phase and XRD results indicate nearly identical peak intensities for the three specimens it seems that all specimens have nearly achieved the maximum amount of possible ferrite phase, which is theoretically ~50 wt.%. It has been reported [20] that the theoretical value of M_s for barium hexaferrite single crystal is 72 emu/g. Therefore, it can be concluded that the measured M_s in this experiment is ~75% of the theoretical value.

In contrast to the M_s values, the H_c values obtained in this work greatly differ for various specimens. The coercivity values (H_c) in addition to crystal structure mainly depend on the size and shape of the particles of magnetic phase. Finer particles and specific shapes (e.g. needles) usually increase the value of H_c [3,5,8,12]. Specimen B represents a quite high value of H_c = 3800 Oe, in comparison to the values reported in the literature for Ba-hexaferrite glass-ceramics in this system.

It can be attributed to the acicular morphology of some ferrite particles present in this specimen (with a mean

Table 4
Magnetic properties obtained under a maximum magnetic field of 20 kOe

Specimen	M_s (emu/g)	H_c (Oe)
B	25	3800
C	27	2800
D	26	3300

particle size of 2.6 μm and an aspect ratio of 6–7) and also the presence of numerous small platelet particles in the size range of 0.1–2.5 μm. On the other hand, specimen C exhibiting the lowest value of H_c = 2800 Oe with the most uniform structure regarding the size and shape of hexaferrite particles with a mean size of ∼0.9 μm. It is known that the critical size of barium hexaferrite particles below which the particles may magnetically be single domain is 0.460 μm [12,17]. Therefore, in this specimen most of particles are multi-domain. Single domain particles may have a marked effect in increasing H_c values, while multi-domain particles usually reduce H_c. In multi-domain particles the processes of magnetization and demagnetization proceed by the relatively easy process of domain wall motion, whereas in single domain particles, (in which formation of domain walls is energetically unfavourable owing to very small sizes of particles). The magnetization and demagnetization proceed by the difficult process of rotation of magnetization vector [1].

On the other hand, a certain degree of interconnectivity is observed in the microstructure of these specimens which may be responsible for lowering of H_c (Fig. 6).

It was initially supposed that the two-stage heat treatment in specimen D might raise the H_c value by reducing the mean particle size of magnetic phase. However, it was proved that although a considerable increase in H_c has occurred in comparison to specimen C (from 2800 to 3300 Oe) but It is still less than the value observed for specimen B. It is suggested that the quite big size of some hexagonal particles is probably responsible for this. Meanwhile in contrast to specimen C, specimens B and D exhibited high amounts of borate phase. It seems that the surface nucleation and inclusion of a nucleation step in the heat treatment schedule in specimens B and D, respectively, have facilitated the formation of the borate phase.

Finally it can be concluded that although the greater tendency of the adopted composition towards surface crystallisation is mainly responsible for finer microstructure and higher H_c values in specimen B, but it is obvious that the relatively broad range of particle sizes in this specimen and still the multi-domain characteristic of most of the particles are not suitable for some applications. On the other hand, it was proved that the inclusion of nucleation step in heat treatment schedule of specimen D has not been successful in producing a uniform microstructure of fine grains. Therefore, in this stage it was decided to add various nucleation agents to this glass composition to provoke heterogeneous nucleation process. Further experimental work is underway in this connection.

4. Conclusions

Formation of amorphous ribbons with $0.35BaO{\cdot}0.35Fe_2O_3{\cdot}0.20B_2O_3{\cdot}0.10SiO_2$ composition and their subsequent crystallisation in the form of bulk glass samples and pressed frits were investigated. DTA results revealed the existence of a marked tendency towards surface crystallisation. The crystallisation processes were carried out at DTA exo-peak temperatures of 722 and 702 °C for bulk and powder specimens, respectively. Both specimens developed $BaFe_{12}O_{19}$ and BaB_2O_4 as the only major crystalline phases after 1 h heat treatment at above temperatures. The powder specimen exhibited the broadest and finest distribution of hexaferrite particles in the form of needles and platelets in the size range of 0.1–2.5 μm and the bulk sample showed a relatively uniform distribution of ferrite platelets in ∼0.9 μm mean size. The nucleation of bulk samples at 527 °C for 1 h prior to the final crystallisation at 722 °C resulted in a bimodal distribution of large well developed hexagonal particles of 14 μm mean diameter and much finer platelets of 0.6 μm mean size.

All specimens exhibited an approximately identical M_s value of 25–27 emu/g. Coercevity values varied between 3800 and 2800 Oe for powder and bulk specimens, respectively. The nucleated bulk samples represented the intermediate value of 3300 Oe. The barium borate phase was formed in the form of spherical particles and irregularly shaped small particles in the bulk and powder specimens, respectively. The one-stage heat treated bulk specimens developed the least amount of borate phase whereas the other specimens showed higher amounts of this phase, proving that its crystallisation rate is mainly controlled by nucleation step.

References

[1] B.T. Shirk, W.R. Buessem, Magnetic properties of barium ferrite formed by crystallisation of glass, J. Am. Ceram. Soc. 53 (1970) 192–196.
[2] O. Kubo, T. Ido, H. Yocoyama, Properties of barium ferrite particles for perpendicular magnetic recording medias, IEEE Trans. Magn. Magn. 18 (1982) 1122–1124.
[3] K. Oda, T. Yoshio, K.O. Oka, Morphology and magnetic properties of $BaFe_{12}O_{19}$ particles prepared by the glass-ceramic method, J. Mater. Sci. Lett. 20 (1985) 876–879.
[4] H. Zagnazi, C. Chaumont, J.C. Bernier, Rules for the preparation of powders by the glass synthesis method—application to barium hexaferrite, J. Solid State Chem. 65 (1986) 370–376.
[5] S. Ram, D. Bahadur, D. Chakravorty, Magnetic glass-ceramics with hexagonal lead ferrites, J. Non-Cryst. Solids 88 (1986) 311–322.
[6] F. Haberey, Proportion of M and W-type hexaferrite particles by the glass crystallisation method on the basis of the pseudo-ternary system Fe_2O_3–BaO–B_2O_3, IEEE Trans. Magn. Magn. 23 (1987) 29–32.
[7] S. Ram, D. Bahadur, D. Chakravorty, Crystallisation of W-type hexagonal ferrites in an oxide glass with As_2O_3 as nucleation catalyst, J. Magn. Mater. 67 (1987) 378–386.
[8] P. Brahma, K. Choudhury, R. Guha, D. Chakravorty, Crystallisation of Ba–M ferrite in a glass with Sb_2O_3 as nucleation catalyst, J. Mater. Sci. Lett. 24 (1989) 540–542.
[9] C.K. Lee, R.F. Speyer, Glass formation and crystallisation of barium ferrite in the Na_2O–BaO–Fe_2O_3–SiO_2 system, J. Mater. Sci. 29 (1994) 1348–1351.
[10] C.K. Lee, R.F. Berta, R.F. Speyer, Effect of Na_2O addition in the crystallisation of barium ferrite from a BaO–B_2O_3–Fe_2O_3 glass, J. Am. Ceram. Soc. 79 (1996) 183–192.

[11] K. Watananabe, K. Hoshi, Crystallisation kinetics of fine barium hexaferrite, $BaFe_{12}O_{19}$ particles in a glass matrix, Phys. Chem. Glasses 40 (1999) 75–78.
[12] L. Rezlescu, E. Rezlescu, P.D. Popa, N. Rezlescu, Fine barium hexaferrite powder prepared by the crystallisation of glass, J. Magn. Magn. Mater. 193 (1999) 288–290.
[13] S.B. Sohn, S.Y. Choi, I.B. Shim, Preparation of Ba-ferrite containing glass-ceramics in $BaO–Fe_2O_3–SiO_2$, J. Magn. Magn. Mater. 239 (2002) 533–536.
[14] P. Görnert, E. Sinn, W. Schüppel, H. Pfeiffer, M. Rösler, T. Schubert, M. Jurisch, R. Selger, Structural and magnetic properties of $BaFe_{12-2x}Co_xTi_xO_{19}$ powder prepared by the glass crystallisation method, IEEE Trans. Magn. 26 (1990) 12–15.
[15] H. Zagnazi, M. Malassis, C. Chaumont, J.C. Bernier, Preparation of cobalt and fluorine-doped barium hexaferrite by the glass synthesis method, J. Am. Ceram. Soc. 73 (1990) 167–169.
[16] V.K. Marghussian, A. Beitollahi, M. Haghi, The effect of SiO_2 and Cr_2O_3 additions on the crystallisation behaviour and magnetic properties of a $B_2O_3–BaO–Fe_2O_3$ glass, Ceram. Int. 29 (2003) 455–462.
[17] S. Ram, D. Chakravorty, D. Bahadur, Effect of nucleating agents on the crystallisation behaviour of barium hexaferrite in a borate glass, J. Magn. Magn. Mater. 62 (1986) 221–232.
[18] H.D. Keith, F.J. Padden Jr., A phenomenological theory of spherulitic crystallisation, J. Appl. Phys. 34 (1963) 2409–2421.
[19] S.W. Freiman, G.X. Onoda Jr., A.G. Pincus, Spherulitic crystallisation in glasses, in: L.L. Hench, S.W. Freiman (Eds.), Advances in Nucleution and Crystallisation in Glasses, American Ceramic Society, Columbus, OH, 1971, pp. 144–150.
[20] B.T. Shirk, W.R. Buessem, Temperature dependence of M_s and k_1 of $BaFe_{12}O_{19}$ and $SrFe_{12}O_{19}$ single crystals, J. Appl. Phys. 40 (1969) 1294–1296.